NANO LETTERS

pubs.acs.org/NanoLett Letter

Near-Field Infrared Nanospectroscopy Reveals Guest Confinement in Metal–Organic Framework Single Crystals

Annika F. Möslein, Mario Gutiérrez, Boiko Cohen, and Jin-Chong Tan*

Cite This: *Nano Lett.* 2020, 20, 7446–7454 Read Online

ACCESS | Metrics & More | Article Recommendations | Supporting Information

ABSTRACT: Metal–organic frameworks (MOFs) can provide exceptional porosity for molecular guest encapsulation useful for emergent applications in sensing, gas storage, drug delivery, and optoelectronics. Central to the realization of such applications, however, is the successful incorporation of a functional guest confined within the host framework. Here, we demonstrate, for the first time, the feasibility of scattering-type scanning near-field optical microscopy (s-SNOM) and nano-Fourier transform infrared (nanoFTIR) spectroscopy, in concert with density functional theory (DFT) calculations to reveal the vibrational characteristics of the Guest@MOF systems. Probing individual MOF crystals, we pinpoint the local molecular vibrations and, thus, shed new light on the host–guest interactions at the nanoscale. Our strategy not only confirms the successful encapsulation of luminescent guest molecules in the porous host framework in single crystals but also further provides a new methodology for nanoscale-resolved physical and chemical identification of wide-ranging framework materials and designer porous systems for advanced applications.

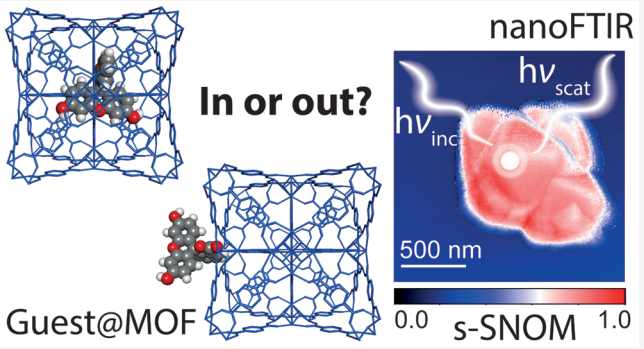

KEYWORDS: *Metal–organic frameworks, infrared nanospectroscopy, host–guest interaction, optical near-field microscopy, single crystal, nanoconfinement*

Downloaded via UNIV OF OXFORD on October 15, 2020 at 14:52:54 (UTC).
See https://pubs.acs.org/sharingguidelines for options on how to legitimately share published articles.

INTRODUCTION

Metal–organic frameworks (MOFs), characterized by their crystalline hybrid structure, are constructed from metal clusters and organic linkers via self-assembly at the molecular level. MOFs exhibit remarkably large internal surface areas, far exceeding those found in conventional porous materials such as zeolites and carbon black.[1] Merging the hybrid nature of MOFs with the ability to precisely tailor the characteristics of the pore yields multifunctional properties, boosting their deployment in emerging technologies ranging from gas storage and catalysis to luminescence, dielectrics, drug delivery, and sensors.[2−6] Due to their potential in prospective optoelectronic and sensing technologies, the research interest in luminescent MOFs has intensified toward accomplishing MOF-based devices for real-world applications.[7−9] In this context, the encapsulation of "guest" functional molecules into the "host" MOF pores is a versatile strategy to engineer the Guest@MOF composite materials with tunable physicochemical properties arising from host–guest interactions.[10,11]

There are, however, outstanding challenges to be addressed to achieve the full potential of Guest@MOF systems. Particularly, it is very plausible that during the *in situ* synthesis or *ex situ* infiltration process the guest molecules are adsorbed onto the external surfaces of MOFs instead of truly being encapsulated inside the pores. Unambiguously proving the latter is not a trivial task. Herein, we confirm—on single crystals—the fundamental encapsulation of luminescent guest molecules (fluorophores) into the framework structures of the MOF host material. Our nanoscale multimodal approach combines fluorescence lifetime imaging microscopy (FLIM) with precise determination of the vibrational dynamics of individual crystals, employing the scattering-type scanning near-field optical microscopy (s-SNOM) integrated with nano-Fourier transform infrared (nanoFTIR) spectroscopy, circumventing the diffraction limit of light.[12] The combination of the latter local-scale techniques enables us to perform single-crystal imaging and nanoscale chemical characterization by simultaneously measuring topography and infrared-active vibrational modes, which yields spectral information spatially resolved down to 20 nm.[13] While interference microscopy and scanning transmission electron microscopy have been used to study crystal diversity with time-resolution[14] and heterodomains of MOFs,[15] respectively, s-SNOM measurements could surpass

Received: July 10, 2020
Revised: August 29, 2020
Published: September 1, 2020

ACS Publications © 2020 American Chemical Society

https://dx.doi.org/10.1021/acs.nanolett.0c02839
Nano Lett. 2020, 20, 7446–7454

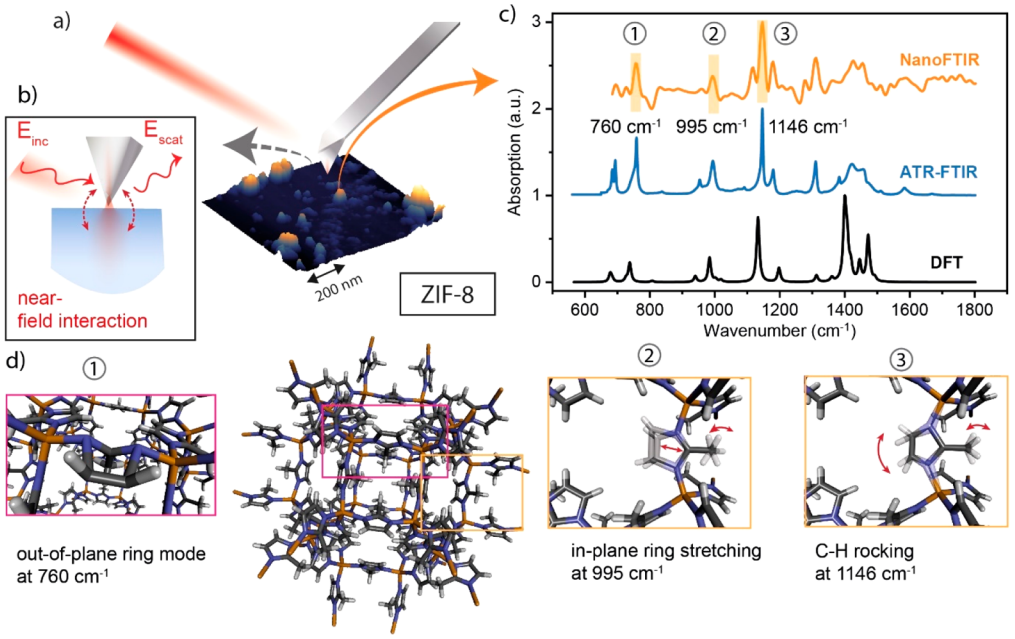

Figure 1. Near-field optical spectroscopy of individual ZIF-8 nanocrystals. (a) Representation of the setup of the s-SNOM measurement stage; the illuminated AFM tip generates a nanofocus on the sample. (b) The near-field interaction between the tip and the sample changes the scattered light from which the local optical properties of the sample are derived. (c) Mid-IR spectra of ZIF-8 crystals obtained via nanoFTIR and ATR-FTIR measurements, compared with the DFT calculations. The DFT spectrum was shifted by a factor of 0.97 to better match the experimental measurements.[21] (d) Characteristic vibrational modes of the ZIF-8 crystal structure: (1) out-of-plane deformation of the mIM ring at 760 cm^{-1}, (2) in-plane stretching of the mIM ring at 995 cm^{-1}, and (3) C−H rocking of the mIM linker at 1146 cm^{-1}.

the spatial resolution of these techniques. The s-SNOM setup employed in this work is based on an atomic force microscope (AFM), where a platinum-coated cantilever tip serves as a topographical and near-field optical probe simultaneously (Figure 1a). Upon illumination, the probe induces an evanescent near-field by acting as a nanoscale light confiner, enhancer, and scatterer, which is key to obtain wavelength-independent resolution (Figure 1b).[16] As the tip polarizes the sample, the optical near-field interaction between the metallic tip and the sample modifies the elastically scattered light. Interferometric detection provides sensitivity to measure the sample's permittivity at a resolution comparable to the dimension of the tip apex.[16] When this signal is Fourier transformed, sample-specific FTIR spectra with a spatial resolution of down to 20 nm are obtained (hereafter we refer to these length scales as "local").[13,17]

For the nanoFTIR method, the tip is operating in tapping mode at its mechanical resonance frequency (Ω = 250 kHz) under illumination from a tunable broadband IR laser. Demodulating the detector signal at higher harmonics of the tip oscillation frequency ($n\Omega$) extracts the near-field interaction from background contributions.[18] Once normalized to a reference signal, this gives the complex-valued near-field contrast, whose imaginary part defines the local nanoFTIR absorption (further details in SI sections 1−2). s-SNOM imaging is achieved via a monochromatic irradiation source instead of a broadband laser. In this case, the illumination wavelength is tuned close to an absorption band of interest to map the material surface on a 2D areal scan. Analogous to nanoFTIR, the scattered light is detected and deconvoluted at higher harmonics of the tip frequency to record the local optical properties through near-field contributions. Optical amplitude and phase now indicate regions of the sample's reflection and absorption at the specific wavelength to derive contrast images with nanoscale resolution.

In this work, we first demonstrate the efficacy of the near-field optical techniques for the physical and chemical characterization of MOF single crystals (ca. 100s nm to 1 μm). As a proof of concept, we measure nanoFTIR absorption spectra from individual crystals of zeolitic imidazolate framework ZIF-8 [$Zn(mIM)_2$; mIM = 2-methylimidazolate],[19] which represents a prototypical imidazole-based MOF with sodalite cage topology. We compare the near-field spectra with far-field FTIR measurements of a bulk sample and with the theoretical spectra of ZIF-8. Subsequently, we demonstrate how to confirm the nanoscale confinement of luminescent dye guest molecules, such as rhodamine B (RhB) or fluorescein, encapsulated in ZIF-8 and UiO-66, where the latter is a prototype of a highly stable zirconium-based framework [$Zr_6O_4(OH)_4(BDC)_6$; BDC = benzene-1,4-dicarboxylate].[20] Specifically, we study the RhB@ZIF-8, RhB@UiO-66, and fluorescein@UiO-66 composite systems, finally validating the Guest@MOF concept.

RESULTS AND DISCUSSION

IR Spectroscopy of MOF Single Crystals. We first demonstrate that the described nanoFTIR method can be employed to probe individual MOF-type crystals. Herein, we compare the vibrational spectra of near-field nanoFTIR experimental measurements of ZIF-8 crystals with far-field attenuated total reflection (ATR-FTIR) measurements and these experiments against *ab initio* quantum mechanical calculations from density functional theory (DFT). The results are shown in Figure 1c. In the mid-IR region, the characteristic peaks at 760, 995, and 1146 cm^{-1} are all fully resolved in the nanoscale measurements. Guided by DFT calculations of ZIF-8,[22] we assign these vibrational bands to the out-of-plane and

https://dx.doi.org/10.1021/acs.nanolett.0c02839
Nano Lett. 2020, 20, 7446−7454

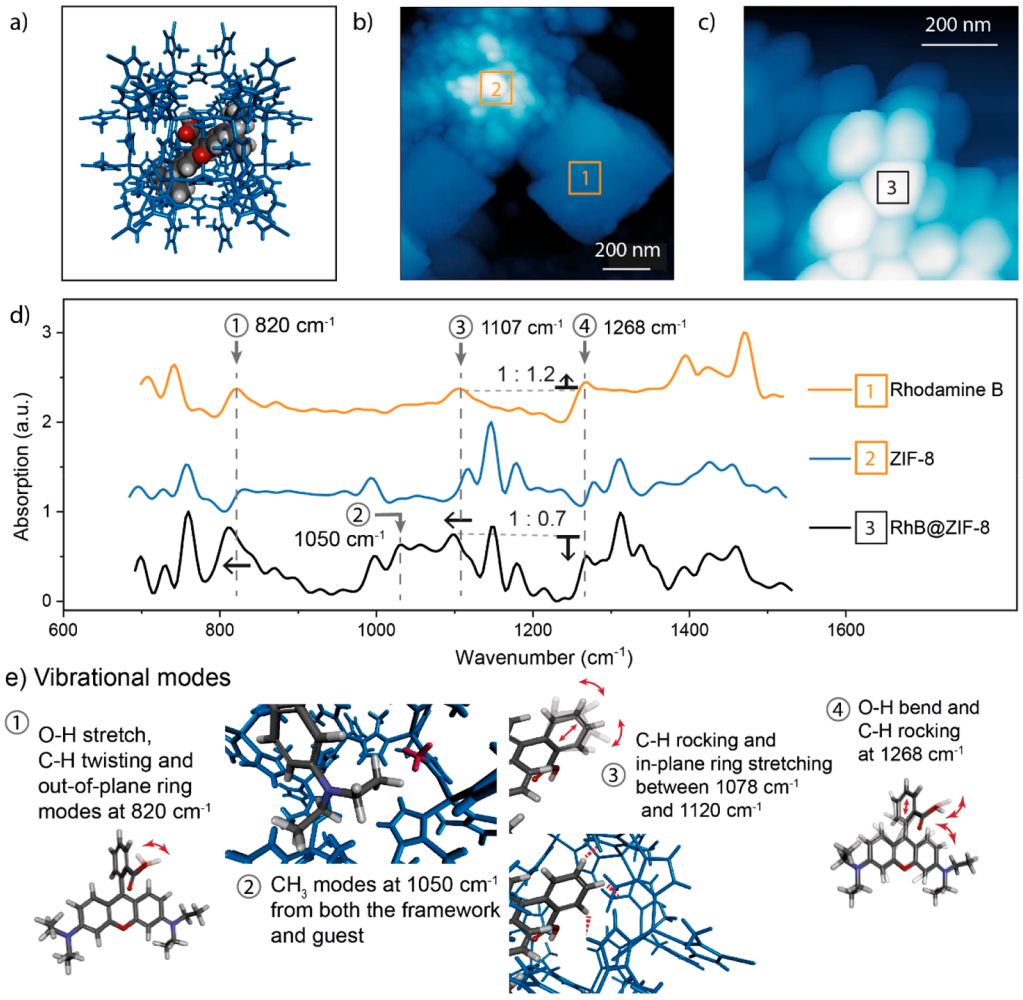

Figure 2. Vibrational analysis of rhodamine B (RhB) and ZIF-8 via nanoFTIR and DFT calculations. (a) Schematic representation of the RhB@ZIF-8 composite, depicting a RhB guest molecule being encapsulated in the pore of the ZIF-8 host framework (in blue). (b) AFM image of the as-synthesized sample containing two distinctive phases, i.e., (1) RhB and (2) ZIF-8, showing the positions where IR spectra were recorded. (c) AFM image of a single-phase sample of ZIF-8 nanocrystals adsorbing RhB. (d) nanoFTIR spectra determined at the designated locations on the AFM image. (e) Vibrational modes of the RhB@ZIF-8 composite illustrating the interactions between the ZIF-8 host framework and the RhB guest.

the in-plane ring stretching modes of the mIM linker, as well as the rocking mode of its C−H bonds, respectively, as illustrated in Figure 1d. Similarly, the in-plane ring bending modes of C−N bonds at 1116 and 1311 cm^{-1}, as well as the symmetric C−N stretching mode at 1445 cm^{-1}, are present in the nanoFTIR spectra.

Indeed, the matching IR spectra demonstrate the capability of nanoFTIR spectroscopy to characterize a MOF-type single crystal; nonetheless, this near-field technique yields minor changes in the IR spectrum. It is worth mentioning that our DFT calculation assumes a defect-free periodic crystal and neglects anharmonicity, while the far-field ATR-FTIR method measures the averaged response of a bulk (polycrystalline) powder material. In contrast, a local scale characterization of individual single crystals is achieved by leveraging nanoFTIR. Here, with a probing depth of ∼20 nm, surface effects might influence the IR spectrum. Close to the crystal boundary, where the framework symmetry is lost, some functional groups are surrounded by voids and air instead of their atomic neighbors assumed in a periodic crystalline structure. Such changes in the atomic environment will affect the strength of the bonds, altering their vibrational frequencies, and as a result, additional peaks and broader peak shapes are observed (Figure 1c). Although subtle alterations in the IR spectrum are observable, they are explained by the nature of experimental surface measurements. In fact, nanoFTIR spectroscopy yields good agreement with established FTIR and DFT methods, thus allowing direct chemical recognition of MOFs through standard FTIR databases; furthermore, it has the unique advantage to directly measure a local IR spectrum reflecting the complex nature of a single MOF crystal whose size is of the order of ∼100 nm.

Host−Guest Interactions at the Nanoscale. Local probing enables a deeper examination of the host−guest interactions in Guest@MOF systems. Crucially, one might ask whether the guest molecule is actually incorporated in the pores of the framework or adsorbed only to its external surface, which, to date, has been a major challenge. Utilizing nanoFTIR and s-SNOM imaging, for the first time, give us the unique opportunity to chemically pinpoint the interaction of the guest molecule at the nanoscale with the MOF host.

Here, we consider an example Guest@MOF system, termed RhB@ZIF-8 (Figure 2a), comprising the luminescent RhB guest in ZIF-8 host, resulting in a fluorescent material potentially useful for optoelectronics and photonic sensors.[23,24] However, the adsorption of RhB in preassembled ZIF-8

https://dx.doi.org/10.1021/acs.nanolett.0c02839
Nano Lett. 2020, 20, 7446−7454

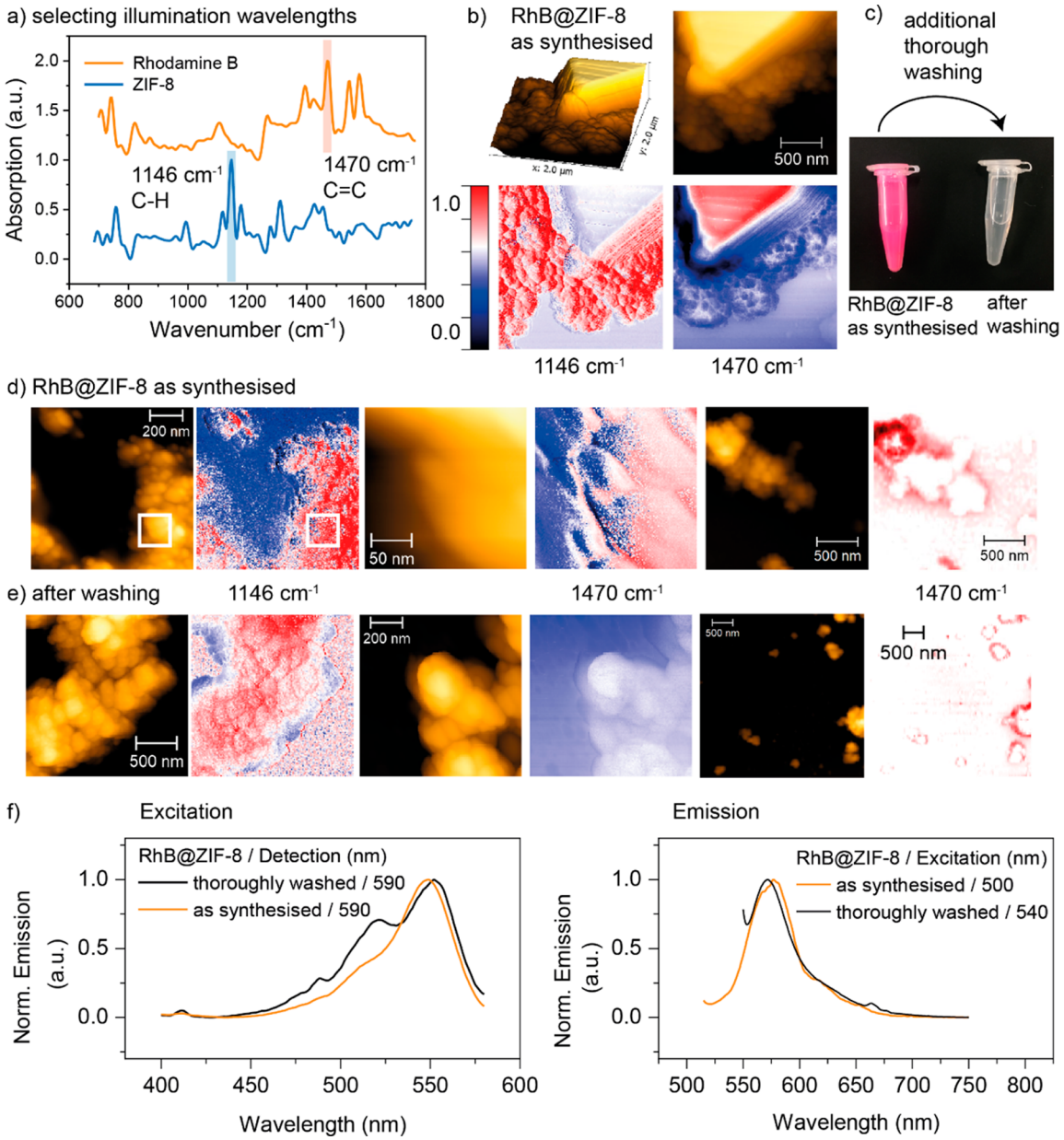

Figure 3. s-SNOM imaging of RhB@ZIF-8. (a) The illumination source was tuned to the characteristic peaks of RhB and ZIF-8. (b) Validation of the contrast images with known, distinguishable material distribution. (c) Samples before and after thorough washing, viewed under daylight. (d) AFM and near-field optical phase imaging of as-synthesized RhB@ZIF-8 with illumination at 1146 cm^{-1}, confirming the presence of ZIF-8, and illumination at 1470 cm^{-1} still revealing RhB on the surface. (e) Near-field optical phase imaging of RhB@ZIF-8 after thorough washing, verifying the complete removal of residual RhB from the sample surface. (f) Normalized excitation and emission spectra of the as-synthesized and thoroughly washed RhB@ZIF-8 (dispersed in acetone) confirming the presence of RhB in both samples. Excitation and detection wavelengths are indicated in the figure.

crystals only leads to surface interactions, since the size of the RhB molecule (13.5 Å) exceeds the window aperture of the ZIF-8 pore (3.4 Å), thus hindering guest infiltration.[25] Therefore, we applied an *in situ* encapsulation of RhB molecules during ZIF-8 formation to synthesize the RhB@ZIF-8 composite (see Methods and Figure S3). Albeit, to isolate the as-synthesized RhB@ZIF-8, several washing steps were performed. AFM imaging revealed different phases with round nanocrystals and micrometer-sized blocks as their distinct morphologies (Figure 2b). Equally, local probing of the features with nanoFTIR spectroscopy yields two significantly different IR spectra. First, the cuboidal block is identified as pure RhB crystals through comparison with the DFT-simulated IR peaks (at 820, 1107, 1268, 1470, and 1576 cm^{-1}, calculated by Gaussian). Second, the frequencies measured at the individual round nanocrystals are matching the IR spectrum of pristine ZIF-8. Consequently, disparate regions of RhB and ZIF-8 are clearly distinguishable by nanoFTIR, where the topography and chemical fingerprint for each constituent material are identifiable without any indication of molecular interaction.

In the third region (Figure 2c), the block crystals of RhB are absent, and the topography resembles the ZIF-8 nanocrystals. Interestingly, probing the individual crystals in this region yields an IR spectrum with characteristic features of both constituent materials (Figure 2d). Although far-field FTIR

https://dx.doi.org/10.1021/acs.nanolett.0c02839
Nano Lett. 2020, 20, 7446−7454

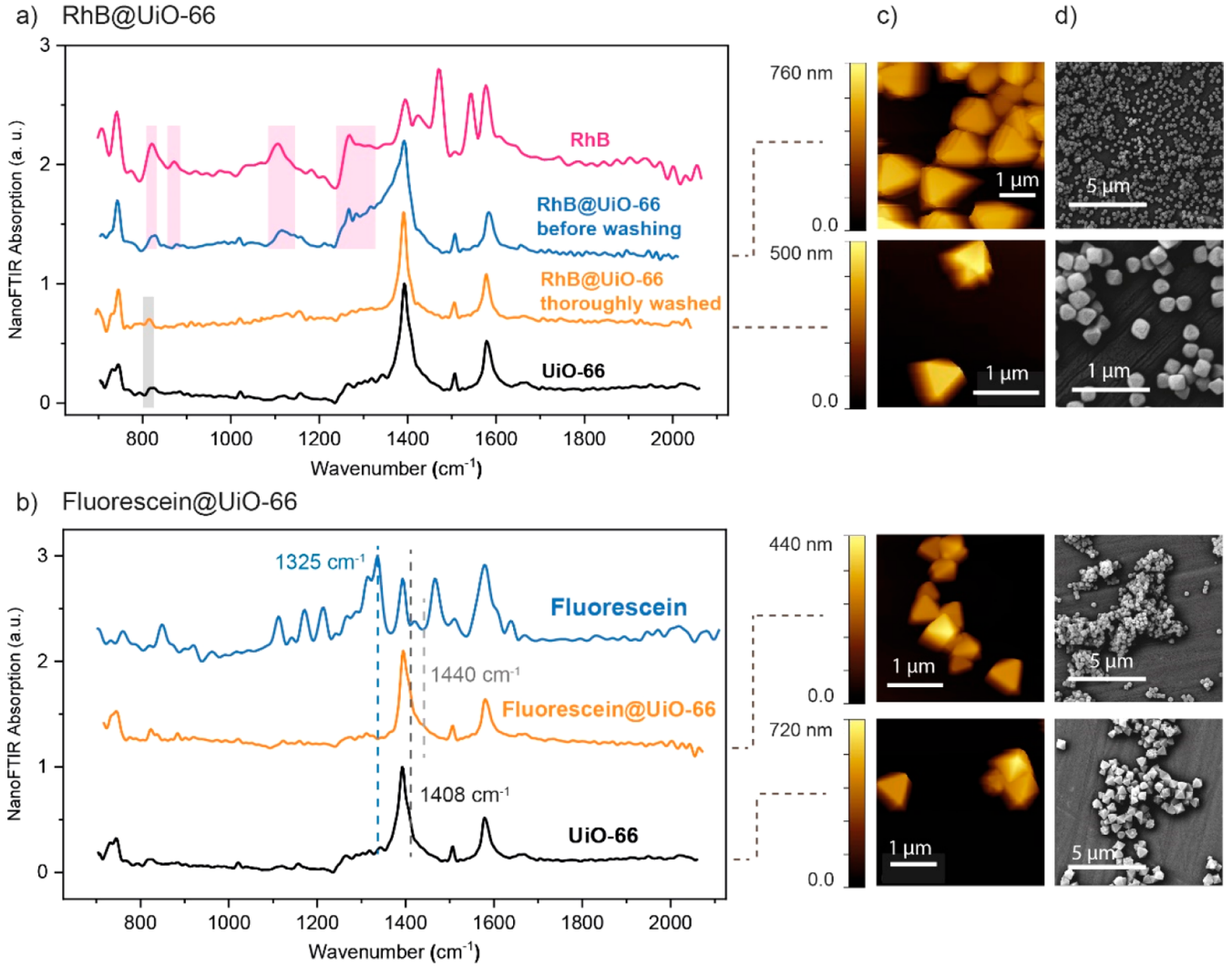

Figure 4. Near-field nanospectroscopy of UiO-66 single crystals with the encapsulated guest RhB and fluorescein, respectively. (a) Near-field IR absorption spectra of RhB, UiO-66, and as-synthesized RhB@UiO-66 composite (without washing the sample) and after thorough washing. (b) The nanoFTIR spectrum of fluorescein@UiO-66 measured on thoroughly washed nanocrystals revealing the absence of fluorescein on the sample surface. Distinguishable wavelengths are selected for subsequent s-SNOM imaging. (c) AFM and (d) SEM images of UiO-66, RhB@UiO-66, and fluorescein@UiO-66 crystals.

measurements may equally lead to a combined IR spectrum, it is worth emphasizing that this is due to the averaged probing over the bulk polycrystalline material without discriminating between the constituent materials present at the local scale. At the measured spot size of 20 nm, in contrast, the superposition of the spectra reveals the concurrent presence of RhB and ZIF-8, leading to the conclusion that the RhB interacts with the ZIF-8 framework due to two reasons. First, all characteristic modes associated with the host framework were identified in the IR spectrum. Second, the vibrational bands assigned to RhB have been modified, revealing host−guest interactions. Considering the O−H group, for instance, with its stretch mode at 820 cm^{-1} experiencing a small shift to lower energies, an interaction between the O−H group of the guest molecule and the host framework is indicated, possibly with the Zn-atoms at defect sites.[25,26] Similarly, the bending mode of the O−H group at 1268 cm^{-1} reveals a change in relative intensity with respect to the peak at 1107 cm^{-1}. We found that the CH_3 vibrations in the region ∼1050 cm^{-1} are reinforced due to superposition. The presence of both materials at a nanoscale spot demonstrates the interaction of RhB with the framework; however, this might be influenced by surface adsorption effects. We also observed reduced energy of the phenyl ring stretching modes in RhB at 1107 and 1118 cm^{-1}, which may indicate guest encapsulation. As the dimensions of the RhB molecule almost completely fill the pore of ZIF-8, upon confinement, the free-space vibrations of the trapped molecules are suppressed.

Confirming the Confinement of RhB in the ZIF-8 Framework. One reason for the observed simultaneous presence of guest and framework material at a spot size of 20 nm may be attributed to surface adhesion. To eliminate any residual RhB from adhering on the surface of ZIF-8 nanocrystals, the synthesized RhB@ZIF-8 material was subjected to a second, more thorough washing process (see Methods). If, despite any dye material being removed from the surface, the luminescent properties of RhB are still observable, then the luminescent guests shall be incorporated. On this basis, the material was thoroughly washed until the sample resembled the white color of pristine ZIF-8 rather than the characteristic pink of RhB (Figure 3c). As verification, the

https://dx.doi.org/10.1021/acs.nanolett.0c02839
Nano Lett. 2020, 20, 7446−7454

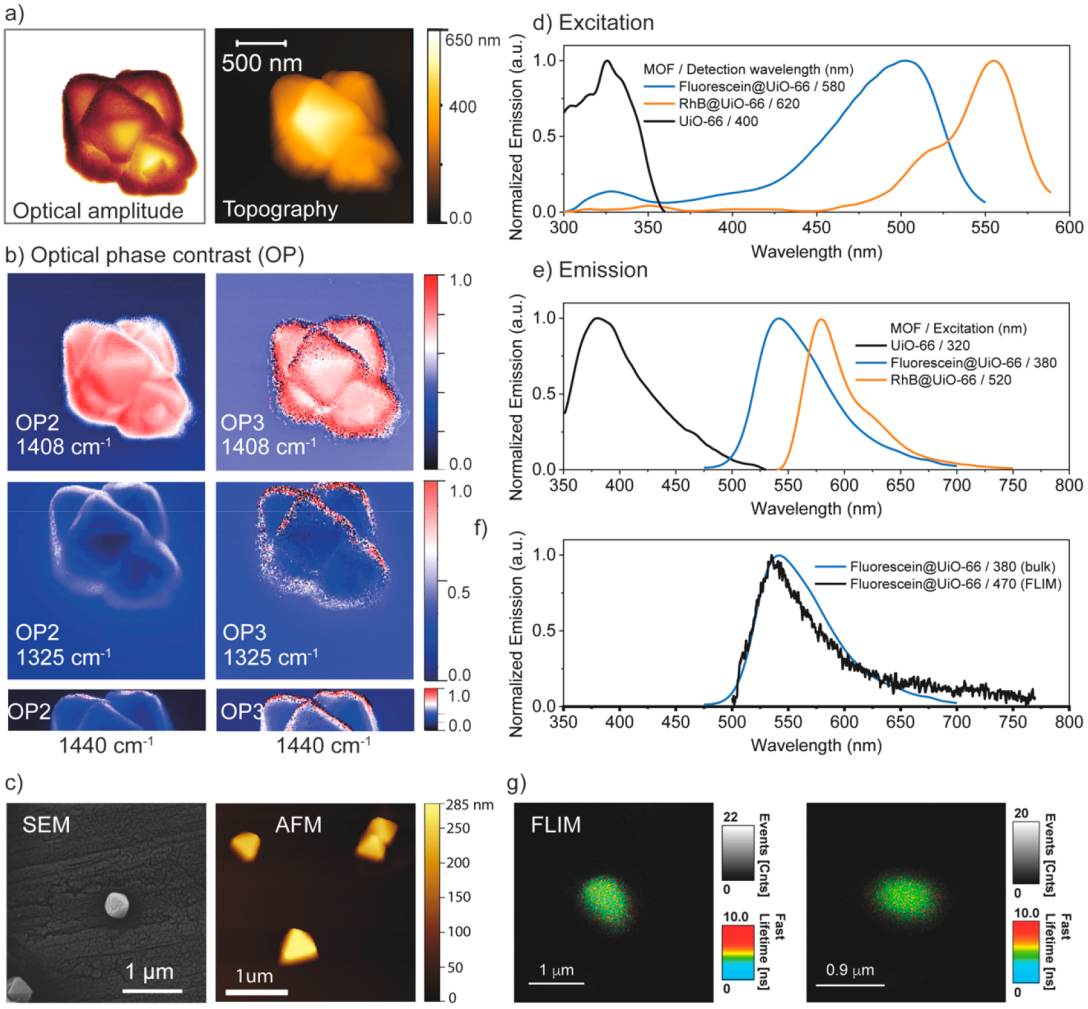

Figure 5. Nanoscale imaging confirming guest encapsulation in UiO-66. (a) Topography and optical amplitude imaging demonstrating the typical size and morphology of the crystals. (b) s-SNOM imaging technique proves that there are no traces of fluorescein on the surface of the UiO-66 crystals. The optical phase images were obtained via illumination at the major absorption peaks of UiO-66 (1408 cm^{-1}) and fluorescein (1325 cm^{-1}) and at a reference position (1440 cm^{-1}), as shown in Figure 4b. (c) SEM and AFM imaging of the individual UiO-66 crystals. (d, e) Excitation and emission spectra of UiO-66 and thoroughly washed Guest@UiO-66 powder samples. Excitation and detection wavelengths are indicated in the figures. (f) Emission spectrum of a single crystal of fluorescein@UiO-66 obtained with a confocal fluorescence microscope compared with the spectrum of powder sample revealing the presence of fluorescein. (g) Fluorescence lifetime imaging microscopy (FLIM) confirming the encapsulation of fluorescein in UiO-66 single crystals, measured under an excitation wavelength of 470 nm.

supernatant of the final washing step was characterized by UV absorption and fluorescence spectroscopy, and since no signal of the dye was obtained, the thorough washing is confirmed (Figure S12). Both the as-synthesized RhB@ZIF-8 (Figure 3d) and the material obtained after thorough washing (Figure 3e) were initially probed using s-SNOM imaging at the illumination wavelength of 1146 cm^{-1}, a characteristic peak of ZIF-8 (Figure 3a), to confirm the presence of ZIF-8 nanocrystals. Upon illumination, only the ZIF-8 crystals absorb IR radiation, represented by the red color in the optical contrast image (Figure 3b), while the RhB block appears transparent like the gold substrate (blue color). Conversely, excitation at 1470 cm^{-1} leads to the inverted contrast due to the strong absorbance of the excited C═C modes of RhB (Figure 3b). Since the surface of the nanocrystals isolated prior to exhaustive washing exhibits regions where the distinctive wavelength for RhB is absorbed, we can unambiguously conclude that RhB is still attached to the surface. After thorough washing, however, no trace of RhB can be found on the surface of the ZIF-8 nanocrystals. The same phenomenon was observed at larger scan areas, where, for clarity, the optical phase contrast is normalized to demonstrate the excess RhB on the RhB@ZIF-8 material before washing. Note that the red contrast in the thoroughly washed material can be assigned to a shadowing effect at the crystal edges (not originating from intrinsic optical properties of the material), because only the areas surrounding the nanocrystals absorb light.

s-SNOM imaging thus indicates the absence of RhB adhered onto the surface of the ZIF-8 nanocrystals (after thorough washing), with the removal of any excess guest material from the sample further confirmed by SEM imaging (Figure S8). Remarkably, the excitation and emission spectra of the thoroughly washed RhB@ZIF-8 composite show the characteristic bands of RhB (Figure 3f). Fluorescence spectroscopic data reveal the presence of the luminescent dye within ZIF-8, which leads to the conclusion that the guest molecule is successfully encapsulated within the framework. This is strong evidence verifying the formation of the RhB@ZIF-8 composite.

Revealing the Guest Encapsulation in UiO-66. To demonstrate the efficacy of the developed methodologies for

https://dx.doi.org/10.1021/acs.nanolett.0c02839
Nano Lett. 2020, 20, 7446−7454

determining the confinement of guest molecules in MOFs, we have employed two novel Guest@MOF systems as case studies, i.e., RhB@UiO-66 and fluorescein@UiO-66 (Figure 4 and Figure S4). We found that the as-synthesized RhB@UiO-66 still exhibits traces of excess guest material on the surface of the nanocrystals probed via nanoFTIR (Figure 4a). Here, the peaks correlating to the characteristic modes of RhB (in the region between 820 and 1268 cm^{-1}) are visible in the nanoFTIR spectrum in addition to the peaks of the pristine UiO-66 crystals (Figure 4a). An exhaustive washing process—again, confirmed by probing the supernatant with UV absorption and fluorescence spectroscopy (Figure S12)—eliminates any unconfined RhB, and thus, the IR spectrum probed at nanoscale resolution on the surface of the crystals only reveals the representative peaks of UiO-66 (Figure 4a). Turning to the fluorescein@UiO-66 system, likewise, after thoroughly removing any excess guest material, the nanocrystals were identified via nanoFTIR as UiO-66 without any sign of fluorescein on the surface (Figure 4b).

AFM and SEM imaging of the thoroughly washed samples demonstrate the homogeneous crystals without any excess guest material on the sample (Figure 4c,d and Figure S9). To further confirm the absence of the guest adhering on the surface (Figure 5a), not only local point spectra but also the surface of the fluorescein@UiO-66 crystals were examined using s-SNOM imaging (Figure 5b). Hereby, tuning the monochromatic irradiation source to the pronounced peak of UiO-66 at 1408 cm^{-1} illustrates the strong absorbance and reflectance of the crystals in comparison with the substrate. Little contrast, on the other hand, was obtained from illumination at 1325 cm^{-1}, a characteristic peak of fluorescein. Although some absorbance can be observed on the edges of the crystals, again, this can be attributed to noise and shadowing because the same phenomenon emerges at a reference wavelength (1440 cm^{-1}), where neither fluorescein nor the UiO-66 material absorbs. Hence, the absence of any guest material adsorbed on the crystal surface is confirmed. As opposed to the surface techniques, where no signal of the guest molecules is detected, the characteristic emission and excitation bands of RhB and fluorescein are clearly identified for RhB@UiO-66 and fluorescein@UiO-66 composites when measuring their photophysical properties via fluorescence spectroscopy (Figure 5d,e).

Finally, to further corroborate the encapsulation of the fluorophores at a single crystal level, the fluorescence lifetime image (FLIM) of fluorescein@UiO-66 was recorded using a confocal fluorescence microscope (see Methods). Figure 5g shows two single-crystal FLIMs, where clearly, the fluorescein molecules are homogeneously distributed within the UiO-66 crystal. Moreover, the emission spectrum (Figure 5f) of these crystals correlates well with the emission of bulk fluorescein@UiO-66, proving that the emission signal is generated by the fluorescein guest molecules. The mean lifetime of the single crystals is a monoexponential decay of $\tau = 3.77 \pm 0.15$ ns (Figure S10), consistent with the lifetime of fluorescein in different solvents.[27−29] This result suggests that fluorescein molecules are isolated in the form of monomers when partitioned by the pores, as the formation of aggregates will give multiexponential decays.[30] The homogeneous distribution of fluorescein molecules in the form of isolated monomers, alongside with the non-observation of fluorescein on the surface of UiO-66 crystals derived from the nanoFTIR experiments, unequivocally proves the encapsulation of the fluorophores into the MOF pores.

CONCLUSIONS

In summary, this first study of individual ZIF-8 and UiO-66 nanocrystals using near-field optical nanospectroscopy yields new understanding about MOFs and their host−guest interactions. We show the capability of the nanoFTIR methodology to characterize individual MOF-type crystals by comparison with established far-field techniques and *ab initio* theoretical calculations. Taking a step further toward precisely unravelling the physical and chemical properties of MOFs, we present the first near-field spectroscopic evidence of host−guest interactions by locally characterizing both constituent materials at a 20 nm irradiation spot. A detailed analysis of the nanocrystals leveraging s-SNOM imaging confirms the absence of any guest material adsorbed on the surface (after thorough washing), while the photophysical properties of the luminescent molecules are still observable. We conclude that the guest molecule is confined in the framework, thus evidencing the Guest@MOF concept. Our findings provide the groundwork to gain a fundamental understanding of the host−guest interactions underpinning hybrid framework materials, further inviting the examination of other porous materials, e.g., covalent organic frameworks, 2D nanosheets,[11] mixed-matrix membranes,[31] and polycrystalline films for sensing devices.[32,33] Confirming the guest encapsulation paves the way to controlling properties at the nanoscale—the key to engineer a multifunctional platform for nanotechnological applications.

ASSOCIATED CONTENT

Supporting Information

The Supporting Information is available free of charge at https://pubs.acs.org/doi/10.1021/acs.nanolett.0c02839.

Synthetic procedures in detail, methods used for materials characterization (PXRD, nanoFTIR spectroscopy, s-SNOM imaging, fluorescence spectroscopy, FLIM, DFT calculations), further details on measuring the local infrared absorption, and additional figures of material characterization (XRD, AFM, SEM, FLIM) (PDF)

AUTHOR INFORMATION

Corresponding Author

Jin-Chong Tan − *Multifunctional Materials & Composites (MMC) Laboratory, Department of Engineering Science, University of Oxford, Oxford OX1 3PJ, United Kingdom;* orcid.org/0000-0002-5770-408X; Email: jin-chong.tan@eng.ox.ac.uk

Authors

Annika F. Möslein − *Multifunctional Materials & Composites (MMC) Laboratory, Department of Engineering Science, University of Oxford, Oxford OX1 3PJ, United Kingdom;* orcid.org/0000-0002-2056-6437

Mario Gutiérrez − *Multifunctional Materials & Composites (MMC) Laboratory, Department of Engineering Science, University of Oxford, Oxford OX1 3PJ, United Kingdom;* orcid.org/0000-0001-9222-3647

Boiko Cohen − *Departamento de Química Física, Facultad de Ciencias Ambientales y Bioquímica, and INAMOL, Universidad*

https://dx.doi.org/10.1021/acs.nanolett.0c02839
Nano Lett. 2020, 20, 7446−7454

de Castilla-La Mancha, 45071 Toledo, Spain; orcid.org/0000-0002-5400-4678

Complete contact information is available at: https://pubs.acs.org/10.1021/acs.nanolett.0c02839

Notes

The authors declare no competing financial interest.

■ ACKNOWLEDGMENTS

A.F.M. thanks the Oxford Ashton Memorial scholarship for a DPhil studentship award. J.C.T. and A.F.M. are thankful to the ERC Consolidator Grant (771575 (PROMOFS)) for funding. B.C. acknowledges support from JCCM, Spain, grant no. SBPLY/19/180501/000212. We would like to acknowledge the use of the University of Oxford Advanced Research Computing (ARC) facility in carrying out this work (10.5281/zenodo.22558). We are grateful to the Research Complex at Harwell (RCaH) for the provision of advanced materials characterization facilities. A.F.M. would like to thank Dr. Cyril Besnard and Prof. Alexander Korsunsky for their help with SEM imaging and neaspec GmbH for the opportunity to perform s-SNOM imaging in Haar, Germany. We also thank Dr. Abhijeet Chaudhari for the provision of the RhB@ZIF-8 samples.

■ REFERENCES

(1) Furukawa, H.; Cordova, K. E.; O'Keeffe, M.; Yaghi, O. M. The chemistry and applications of metal-organic frameworks. *Science* **2013**, *341* (6149), 1230444.

(2) Zhu, L.; Liu, X. Q.; Jiang, H. L.; Sun, L. B. Metal-Organic Frameworks for Heterogeneous Basic Catalysis. *Chem. Rev.* **2017**, *117* (12), 8129−8176.

(3) Horcajada, P.; Gref, R.; Baati, T.; Allan, P. K.; Maurin, G.; Couvreur, P.; Ferey, G.; Morris, R. E.; Serre, C. Metal-organic frameworks in biomedicine. *Chem. Rev.* **2012**, *112* (2), 1232−1268.

(4) Li, B.; Wen, H. M.; Zhou, W.; Chen, B. Porous Metal-Organic Frameworks for Gas Storage and Separation: What, How, and Why? *J. Phys. Chem. Lett.* **2014**, *5* (20), 3468−3479.

(5) Lustig, W. P.; Mukherjee, S.; Rudd, N. D.; Desai, A. V.; Li, J.; Ghosh, S. K. Metal-organic frameworks: functional luminescent and photonic materials for sensing applications. *Chem. Soc. Rev.* **2017**, *46* (11), 3242−3285.

(6) Ryder, M. R.; Zeng, Z.; Titov, K.; Sun, Y.; Mahdi, E. M.; Flyagina, I.; Bennett, T. D.; Civalleri, B.; Kelley, C. S.; Frogley, M. D.; Cinque, G.; Tan, J.-C. Dielectric Properties of Zeolitic Imidazolate Frameworks in the Broad-Band Infrared Regime. *J. Phys. Chem. Lett.* **2018**, *9* (10), 2678−2684.

(7) Kaur, H.; Sundriyal, S.; Pachauri, V.; Ingebrandt, S.; Kim, K.-H.; Sharma, A. L.; Deep, A. Luminescent metal-organic frameworks and their composites: Potential future materials for organic light emitting displays. *Coord. Chem. Rev.* **2019**, *401*, 213077.

(8) Stassen, I.; Burtch, N.; Talin, A.; Falcaro, P.; Allendorf, M.; Ameloot, R. An updated roadmap for the integration of metal-organic frameworks with electronic devices and chemical sensors. *Chem. Soc. Rev.* **2017**, *46* (11), 3185−3241.

(9) Gutiérrez, M.; Martín, C.; Van der Auweraer, M.; Hofkens, J.; Tan, J. C. Electroluminescent Guest@MOF Nanoparticles for Thin Film Optoelectronics and Solid-State Lighting. *Adv. Opt. Mater.* **2020**, *8*, 2000670.

(10) Allendorf, M. D.; Foster, M. E.; Leonard, F.; Stavila, V.; Feng, P. L.; Doty, F. P.; Leong, K.; Ma, E. Y.; Johnston, S. R.; Talin, A. A. Guest-Induced Emergent Properties in Metal-Organic Frameworks. *J. Phys. Chem. Lett.* **2015**, *6* (7), 1182−1195.

(11) Chaudhari, A. K.; Kim, H. J.; Han, I.; Tan, J. C. Optochemically Responsive 2D Nanosheets of a 3D Metal-Organic Framework Material. *Adv. Mater.* **2017**, *29* (27), 1701463.

(12) Knoll, B.; Keilmann, F. Near-field probing of vibrational absorption for chemical microscopy. *Nature* **1999**, *399*, 134−137.

(13) Huth, F.; Govyadinov, A.; Amarie, S.; Nuansing, W.; Keilmann, F.; Hillenbrand, R. Nano-FTIR absorption spectroscopy of molecular fingerprints at 20 nm spatial resolution. *Nano Lett.* **2012**, *12* (8), 3973−3978.

(14) Remi, J. C. S.; Lauerer, A.; Chmelik, C.; Vandendael, I.; Terryn, H.; Baron, G. V.; Denayer, J. F.; Kärger, J. The role of crystal diversity in understanding mass transfer in nanoporous materials. *Nat. Mater.* **2016**, *15* (4), 401−406.

(15) Collins, S. M.; Kepaptsoglou, D. M.; Butler, K. T.; Longley, L.; Bennett, T. D.; Ramasse, Q. M.; Midgley, P. A. Subwavelength Spatially Resolved Coordination Chemistry of Metal-Organic Framework Glass Blends. *J. Am. Chem. Soc.* **2018**, *140* (51), 17862−17866.

(16) Keilmann, F.; Hillenbrand, R. Near-field microscopy by elastic light scattering from a tip. *Philos. Trans. R. Soc., A* **2004**, *362* (1817), 787−805.

(17) Zenhausern, F.; Martin, Y.; Wickramasinghe, H. K. Scanning interferometric apertureless microscopy: Optical imaging at 10 angstrom resolution. *Science* **1995**, *269*, 1083−1085.

(18) Govyadinov, A. A.; Amenabar, I.; Huth, F.; Carney, P. S.; Hillenbrand, R. Quantitative Measurement of Local Infrared Absorption and Dielectric Function with Tip-Enhanced Near-Field Microscopy. *J. Phys. Chem. Lett.* **2013**, *4* (9), 1526−1531.

(19) Tan, J.-C.; Civalleri, B.; Lin, C.-C.; Valenzano, L.; Galvelis, R.; Chen, P.-F.; Bennett, T. D.; Mellot-Draznieks, C.; Zicovich-Wilson, C. M.; Cheetham, A. K. Exceptionally Low Shear Modulus in a Prototypical Imidazole-Based Metal-Organic Framework. *Phys. Rev. Lett.* **2012**, *108* (9), 095502.

(20) Cavka, J. H.; Jakobsen, S.; Olsbye, U.; Guillou, N.; Lamberti, C.; Bordiga, S.; Lillerud, K. P. A New Zirconium Inorganic Building Brick Forming Metal Organic Frameworks with Exceptional Stability. *J. Am. Chem. Soc.* **2008**, *130* (42), 13850−13851.

(21) Rauhut, G.; Pulay, P. Transferable Scaling Factors for Density Functional Derived Vibrational Force Fields. *J. Phys. Chem.* **1995**, *99* (10), 3093−3100.

(22) Ryder, M. R.; Civalleri, B.; Bennett, T. D.; Henke, S.; Rudic, S.; Cinque, G.; Fernandez-Alonso, F.; Tan, J. C. Identifying the role of terahertz vibrations in metal-organic frameworks: from gate-opening phenomenon to shear-driven structural destabilization. *Phys. Rev. Lett.* **2014**, *113* (21), 215502.

(23) Zhang, Y. Q.; Wu, X. H.; Mao, S.; Tao, W. Q.; Li, Z. Highly luminescent sensing for nitrofurans and tetracyclines in water based on zeolitic imidazolate framework-8 incorporated with dyes. *Talanta* **2019**, *204*, 344−352.

(24) Chaudhari, A. K.; Tan, J. C. Dual-Guest Functionalized Zeolitic Imidazolate Framework-8 for 3D Printing White Light-Emitting Composites. *Adv. Opt. Mater.* **2020**, *8* (8), 1901912.

(25) Chin, M.; Cisneros, C.; Araiza, S. M.; Vargas, K. M.; Ishihara, K. M.; Tian, F. Rhodamine B degradation by nanosized zeolitic imidazolate framework-8 (ZIF-8). *RSC Adv.* **2018**, *8* (47), 26987−26997.

(26) Zhang, C.; Han, C.; Sholl, D. S.; Schmidt, J. R. Computational Characterization of Defects in Metal-Organic Frameworks: Spontaneous and Water-Induced Point Defects in ZIF-8. *J. Phys. Chem. Lett.* **2016**, *7* (3), 459.

(27) Zhang, X. F.; Zhang, J.; Liu, L. Fluorescence properties of twenty fluorescein derivatives: lifetime, quantum yield, absorption and emission spectra. *J. Fluoresc.* **2014**, *24* (3), 819−26.

(28) Magde, D.; Rojas, G. E.; Seybold, P. G. Solvent Dependence of the Fluorescence Lifetimes of Xanthene Dyes. *Photochem. Photobiol.* **1999**, *70* (5), 737−744.

(29) Martin, M. M.; Lindqvist, L. The pH dependence of fluorescein fluorescence. *J. Lumin.* **1975**, *10* (6), 381−390.

(30) Hungerford, G.; Benesch, J.; Mano, J. F.; Reis, R. L. Effect of the labelling ratio on the photophysics of fluorescein isothiocyanate (FITC) conjugated to bovine serum albumin. *Photochem. Photobiol. Sci.* **2007**, *6* (2), 152−158.

(31) Dechnik, J.; Sumby, C. J.; Janiak, C. Enhancing Mixed-Matrix Membrane Performance with Metal-Organic Framework Additives. *Cryst. Growth Des.* **2017**, *17* (8), 4467−4488.
(32) Yuan, H.; Li, N.; Linghu, J.; Dong, J.; Wang, Y.; Karmakar, A.; Yuan, J.; Li, M.; Buenconsejo, P. J. S.; Liu, G.; Cai, H.; Pennycook, S. J.; Singh, N.; Zhao, D. Chip-Level Integration of Covalent Organic Frameworks for Trace Benzene Sensing. *ACS Sens.* **2020**, *5* (5), 1474−1481.
(33) Stassen, I.; Styles, M.; Van Assche, T.; Campagnol, N.; Fransaer, J.; Denayer, J.; Tan, J.-C.; Falcaro, P.; De Vos, D.; Ameloot, R. Electrochemical Film Deposition of the Zirconium Metal-Organic Framework UiO-66 and Application in a Miniaturized Sorbent Trap. *Chem. Mater.* **2015**, *27* (5), 1801−1807.

https://dx.doi.org/10.1021/acs.nanolett.0c02839
Nano Lett. 2020, 20, 7446−7454